Dynamical coupling in Pb(Zr,Ti)O_{3} solid solutions from first principles

Dawei Wang, Jeevaka Weerasinghe, L. Bellaiche, and Jirka Hlinka

Phys. Rev. B **83**, 020301 — Published 13 January 2011

DOI: 10.1103/PhysRevB.83.020301

Dynamical Coupling in $Pb(Zr,Ti)O_3$ Solid Solutions From First Principles

Dawei Wang, Jeevaka Weerasinghe, and L. Bellaiche
Physics department, University of Arkansas, Fayetteville, Arkansas 72701, USA

Jirka Hlinka
Institute of Physics, Academy of Sciences of the Czech Republic, Na Slovance 2, 18221 Prague 8, Czech Republic

A first-principles-based approach is developed to model dynamical coupling between different degrees of freedom in the terahertz frequency range, at any temperature. Such approach is applied to $Pb(Zr,Ti)O_3$ alloys, that exhibit both ferroelectric (FE) and antiferrodistortive (AFD) motions. It reproduces very well the existence of *two* modes (rather than the single $E(1TO)$ soft mode) in the $50-75\,cm^{-1}$ range for temperatures smaller than $\simeq 200\,K$. It also provides an insight into the existence of these two modes, that originates from the coupling between long-range-ordered FE and AFD motions. The proposed scheme is further used to reveal a field-induced *anticrossing* involving FE and AFD degrees of freedom.

PACS numbers: 63.20.-e,63.20.K-,77.22.Ch,77.55.hj

Ferroelectric (FE) and related materials are of great importance for many device applications[1]. For some of these applications and for fundamental reasons, the dynamical properties of these materials need to be determined and understood, especially when realizing that surprises can be in store when they are investigated[2–9]. For instance, some recent studies discovered that $BaTiO_3$ has two (rather than one, as believed for more than 30 years) modes contributing to its dielectric response in the THz range, both in the paraelectric and FE tetragonal phases[2,3]. Similarly, multiferroics (that are materials simultaneously possessing electric and magnetic degrees of freedom) were found to exhibit additional dielectric or Raman peaks in the GHz-THz regime, because of coupling between long-range-ordered electric and magnetic dipoles[4–6]. Such latter peaks are termed electromagnons and are currently attracting much interest. Interestingly, the electric polarization can also dynamically couple with *other* degrees of freedom to give rise to additional peaks that appear in the dielectric or Raman spectra. One example of such degrees of freedom is the antiferrodistortive (AFD) motion, that corresponds to the tilting of the oxygen octahedra. For example, the so-called structural mode (that can be thought as the soft-mode of AFD motions) of $SrTiO_3$ interacts with a polar mode, leading to its observation in the complex dielectric or Raman spectra[10,11] below a critical temperature (below which the structural phase *simultaneously* exhibits *long-range-ordered* tilting of the oxygen octahedra and a spontaneous polarization). It is also believed[12,13] that the additional mode appearing below $\simeq 200\,K$ in the Raman spectra of one of the most important ferroelectrics to date – that is $Pb(Zr,Ti)O_3$ (PZT) – originates from a dynamical coupling between FE and AFD motions.

Being able to acquire an insight into these additional dielectric or Raman peaks is of large importance, since they affect various properties at certain frequencies. One may also wonder if other dynamical phenomena, which also involve the coupling between different degrees of freedom, remain to be discovered. Ideally, addressing such issues would require a computational *ab-initio* scheme with the capability of accurately predicting the consequence of *dynamical coupling* in ferroelectrics at finite temperatures and in the GHz-THz range.

The main goals of this Rapid Communication are four-fold: (1) to demonstrate that it is possible to develop such a scheme; (2) to apply it to PZT to prove its accuracy; (3) to gain a deeper knowledge into the additional peak that has been reported in Refs [12,13] (and that, as we found, does indeed originate from the coupling between FE and AFD motions); (4) to further use the proposed technique to reveal an electric-field-induced anticrossing involving FE and AFD degrees of freedom in PZT.

Practically, we want to simulate finite-temperature dynamical properties of a disordered $Pb(Zr_{0.55}Ti_{0.45})O_3$ solid solution, including those related to FE and AFD degrees of freedom (as well as their couplings). For that, we first take advantage of the effective Hamiltonian scheme of Ref. [14]. The total energy of the system is thus written as

$$\begin{aligned} E_{\rm tot} =& E_{\rm FE}\left(\{\boldsymbol{u}_i\},\{\boldsymbol{v}_i\},\eta_H,\{\sigma_j\}\right) \\ &+ E_{\text{AFD-C}}\left(\{\boldsymbol{u}_i\},\{\boldsymbol{\omega}_i\},\{\boldsymbol{v}_i\},\eta_H,\{\sigma_j\}\right), \end{aligned} \tag{1}$$

where $\boldsymbol{u}_i$ denotes the local soft mode in the unit cell i (which is directly proportional to the electric dipole centered on that cell and is associated with the lowest optical phonon branch), and $\boldsymbol{\omega}_i$ is a vector whose direction is the axis about which the oxygen octahedron of cell i tilts while its magnitude provides the angle of such tilting. $\{\boldsymbol{v}_i\}$ are related to the inhomogeneous strain variables inside each cell[15,16]. η_H is the homogeneous strain tensor, and $\{\sigma_j\}$ characterizes the atomic configuration. $E_{\rm FE}$ gathers the energy terms solely involving the soft mode, strain and their

mutual couplings[17], while $E_{\text{AFD-C}}$ includes the AFD motions and their interactions with the electric dipoles and strain[14]. In particular, one term of $E_{\text{AFD-C}}$ that is relevant to the present study is the interaction energy between the FE and AFD motions, which is given by:

$$E_{\text{AFD-FE}} = \sum_i \sum_{\alpha,\beta,\gamma,\delta} D_{\alpha\beta\gamma\delta}\omega_{i,\alpha}\omega_{i\beta}u_{i\gamma}u_{i,\delta}, \tag{2}$$

where i runs over all the unit cells and $\alpha, \beta, \gamma, \delta$ denote Cartesian components – with the x-, y- and z-axes being chosen along the pseudo-cubic [100], [010] and [001] directions, respectively. The $D_{\alpha\beta\gamma\delta}$ matrix elements quantify the couplings between FE and AFD degrees of freedom, and are extracted from local-density-approximation (LDA) calculations[18,19] – like all the parameters entering Eq. (1).

In order to obtain dynamical properties for any temperature, the total energy of this effective Hamiltonian scheme is then incorporated into a *Molecular Dynamics* (MD) technique. This contrasts with Ref. [14] that used E_{tot} within a *Monte-Carlo* (MC) approach. These MD and MC simulations give similar *static* properties. In particular, for the chosen Ti composition of 45%, a cubic paraelectric phase is found for temperatures above $\sim 700\,\text{K}$ and a $R3m$ phase in which the polarization points along a $\langle 111 \rangle$ direction exists between the Curie temperature $T_C \sim 700\,\text{K}$ and another critical temperature $\sim 200\,\text{K}$. Below such latter temperature, a $R3c$ state occurs, in which the oxygen octahedra tilt, in a long-range fashion, about the same $\langle 111 \rangle$ direction (with neighboring oxygen octahedra rotating in antiphase) and coexist with the electrical polarization. These predictions are all in good agreement with experiments for Ti compositions associated with the rhombohedral side of the morphortropic phase boundary[20–22]. One practical aspect of our presently developed MD simulations is to determine the moment of inertia associated with the oxygen octahedra, as well as the mass associated with the local soft modes, that appear in the Newton's equations of motions. Such determination is accomplished by performing phonon calculations within LDA. More precisely, we adjust these moment of inertia and mass until the frequencies of some modes predicted by the developed technique at small temperature agree with those given by LDA.

One particularly important advantage of the proposed MD scheme is that *two* different complex responses can be computed in the GHz-THz regime at any temperature, via the following equations[2,23]:

$$\begin{aligned}
\varepsilon_{\alpha\beta}(\nu) - 1 =& \frac{1}{\varepsilon_0 V k_B T}\left[\langle d_\alpha(t) d_\beta(t)\rangle + \right. \\
& \left. i2\pi\nu \int_0^\infty dt e^{i2\pi\nu t}\left\langle d_\alpha(t)\, d_\beta(0)\right\rangle\right] \\
\varepsilon^{\text{AFD}}_{\alpha\beta}(\nu) - 1 =& \frac{1}{\varepsilon_0 V k_B T}\left[\left\langle \omega^R_\alpha(t)\omega^R_\beta(t)\right\rangle + \right. \\
& \left. i2\pi\nu \int_0^\infty dt e^{i2\pi\nu t}\left\langle \omega^R_\alpha(t)\,\omega^R_\beta(0)\right\rangle\right]
\end{aligned} \tag{3}$$

where ν is the frequency while α and β define Cartesian components. $\boldsymbol{d}(t)$ and $\boldsymbol{\omega}^R(t)$ are the dipole moment and the order parameter vector associated with the AFD motions at the R-point of the cubic Brillouin zone[14,29] at time t, respectively. $\varepsilon_{\alpha\beta}(\nu)$ is the complex dielectric response[2,3] while $\varepsilon^{\text{AFD}}_{\alpha\beta}(\nu)$ can be thought as the response of $\boldsymbol{\omega}^R(t)$ to its *ac* conjugate field (that is a time-dependent staggered field[24]). Practically, each peak found by our simulations in the spectra of $\varepsilon(\nu)$ and $\varepsilon^{\text{AFD}}(\nu)$ is fitted by a classical harmonic oscillator $S\nu_r^2/\left(\nu_r^2 - \nu^2 + i\nu\gamma\right)$, where ν_r, γ and S are the resonant frequency, damping constant, and strength of the oscillator, respectively. The fact that our simulations provide (unlike Ref. [2]) $\varepsilon^{\text{AFD}}(\nu)$, in addition to $\varepsilon(\nu)$, allows to extract dynamical properties that are difficult to access or interpret experimentally. For instance and as we will see below, the resonant frequency of the AFD distortions can be easily determined at any temperature, and the effect of coupling between FE and AFD degrees of freedom on dynamical properties can be seen and understood. Technically, we first run 10^5 MD steps of NPT simulations on a $12 \times 12 \times 12$ supercell (8640 atoms) to equilibrate the system at a chosen temperature and pressure. Then, the equilibration of the system within an NVE ensemble is performed through 10^5 MD steps. Subsequent 4.3×10^6 NVE steps are performed to obtain the time-resolved physical properties of the system.

Fig. 1 shows the temperature dependence of the resonant frequency, ν_r, as well as the electric dipole spectral weight[4], $S\nu_r^2$, for the lowest-in-frequency dielectric peaks obtained in our simulations. Just below the Curie temperature T_C, the lowest-in-frequency peak corresponds to the well-known $E\,(1\text{TO})$ mode (to be denoted by E, in the following). Such mode represents dipolar oscillations *perpendicular* to the spontaneous polarization. Fig. 1 (a) reveals that, for temperatures below T_C, the resonant frequency of the E mode obeys rather well the relation $\nu_r = C\,|T - T_C|^{1/2}$, with $C = 2.24\,\text{cm}^{-1}\text{K}^{-1/2}$. Similarly, the resonant frequency of the lowest optical mode also follows this square-root law (but with $C = 2.62\,\text{cm}^{-1}\text{K}^{-1/2}$) for $T > T_C$. Note also that the predicted frequency of the E mode is around

$49\,\mathrm{cm}^{-1}$ at room temperature, which agrees rather well with the measured value of $60\,\mathrm{cm}^{-1}$ in $Pb(Zr_{0.55}Ti_{0.45})O_3$ solid solution[25].

Figs. 1 and 2 also reveal that *two* peaks, rather than a single $E(1\mathrm{TO})$ peak, exist in the $50-75\,\mathrm{cm}^{-1}$ range for temperatures *below* $\simeq 200\,K$ – which is the critical temperature at which the $R3m$ to $R3c$ phase transition occurs. These two peaks are denoted as $E^{(1)}$ and $E^{(2)}$ in the following. Interestingly, the Raman experiments of Refs. [12,13] previously indeed reported the existence of two modes exactly within this frequency range, and only for temperature below the $R3m$-$R3c$ transition. Ref. [12] further determined that the upper mode significantly increases its frequency as the temperature decreases while the lower mode only very slightly increases its frequency around $58\,\mathrm{cm}^{-1}$ when the system is cooled down. The predictions shown in Figs 1 and 2 are in excellent agreement with all these experimental findings. Reference [12] also believed that these two modes have $E(\mathrm{TO})$ symmetry and that the lower mode originates from the zone-boundary AFD mode.

Let us turn to the insight provided by our simulations, to check such beliefs and to better understand the reason behind the existence of the $E^{(1)}$ and $E^{(2)}$ modes. Computing the complex dielectric responses in a basis in which the new z-axis is parallel to the polarization reveals that $E^{(1)}$ and $E^{(2)}$ indeed have $E(\mathrm{TO})$ symmetry – i.e., they both correspond to oscillations of the electric dipoles *perpendicularly* to the spontaneous polarization. Moreover, the sum of the electric dipole spectral weights of the $E^{(1)}$ and $E^{(2)}$ modes just below $\simeq 200\,\mathrm{K}$ is nearly equal to that of the E mode just above 200 K [see Fig. 1 (b)]. Such fact hints towards an interaction between the E mode and another dynamical quantity as the culprit for the existence of the $E^{(1)}$ and $E^{(2)}$ vibrations. In order to prove that such other quantity are the AFD distortions, Fig. 2 (c) displays $\varepsilon^{\mathrm{AFD}}(\nu)$ at different temperatures. One can clearly see that the AFD degrees of freedom have *two* natural frequencies in the $50-75\,\mathrm{cm}^{-1}$ range for any temperature below 200K[30], that exactly coincide with the frequencies of the $E^{(1)}$ and $E^{(2)}$ modes. On the other hand, only a single frequency around $\sim 50\,\mathrm{cm}^{-1}$ can be found for the AFD dynamics above 200K, as indicated by Fig. 1(a) and 2(c). Such findings imply that, in the $R3c$ phase, the fluctuations of the AFD degrees of freedom become coupled with the transverse fluctuations of the FE degrees of freedom. The AFD mode acquires some polarity due to this coupling – which explains why it can now be seen in the dielectric spectra (as the $E^{(1)}$ mode) below 200K– while the "usual" E dielectric mode loses some polar character due to that coupling (which explains why the electric dipole spectral weight of $E^{(2)}$ decreases below 200K, see Fig. 1 (b)). In other words, $E^{(1)}$ originates from the AFD motions (as correctly guessed by Ref. [12]) once these motions are allowed to dynamically couple with the FE distortions[31] – that is once the AFD and FE degrees of freedoms both adopt a long-range order[10,11]. $E^{(2)}$ is the remaining signature of the original E mode. We have also numerically find that the $E^{(1)}$ and $E^{(2)}$ modes both mostly originate from the coupling between the E polar mode and the oscillations of the AFD motions *perpendicular* to the polarization's direction.

Let us now use our scheme to simulate the effect of a *dc* electric field applied along the polarization direction on the $E^{(1)}$ and $E^{(2)}$ modes. Figs. 3(a) and (b) show the resonant frequencies and the relative square of the oscillator strengths (extracted from the dielectric responses) of these two modes versus the magnitude of the electric field at 10K. Such figures reveal a "textbook" example of a so-called anticrossing[28]: the $E^{(1)}$ and $E^{(2)}$ modes exchange their character as the field increases (i.e., the $E^{(1)}$ mode becomes less polar while the $E^{(2)}$ modes gains significant polarity) while their frequencies never cross. We are not aware of any previously reported field-induced dynamical anticrossing involving FE and AFD degrees of freedom. Note, however, that such anticrossing can be expected on symmetry grounds since $E^{(1)}$ and $E^{(2)}$ have the same symmetry – namely, they are both $E(\mathrm{TO})$ modes.

In summary, we developed a first-principles-based technique that accurately reproduces, and leads to an insight into, reported dynamical features (at finite temperature and in the GHz-THz range) that are related to coupling between FE and AFD motions. It can also provide predictions of dynamical effects involving such coupling. Interestingly, Eq. (3) can also be put in use in other first-principles-based methods (such as the bond valence[9]) for studying dynamics of materials exhibiting coupled FE and AFD degrees of freedom. Moreover, our proposed scheme can serve as a basis for predicting dynamical properties of systems (such as $BiFeO_3$) that not only exhibit couplings between ferroelectric and antiferrodistortive motions, but also between ferroelectric and other degrees of freedom (such as magnetic dipoles). We thus hope that the present work will deepen the knowledge of the important fields of ferroelectrics and dynamics.

We thank E. Buixaderas, G. Geneste, S. Kamba, I. Ponomareva and S. Prosandeev for useful discussions. This work is mostly supported by the DOE grant DE-SC0002220. We also acknowledge support from ONR grants N00014-08-1-0915 and N00014-07-1-0825 (DURIP), NSF grants DMR 0701558 and DMR-0080054 (C-SPIN). Some computations were made possible thanks to the MRI NSF grant 0722625.

[1] K. Uchino, *Piezoelectric Actuators and Ultrasonic Motors*, Electronic Materials: Science & Technology (Springer; 1 edition, 1996).
[2] I. Ponomareva, L. Bellaiche, T. Ostapchuk, J. Hlinka, and J. Petzelt, Phys. Rev. B **77**, 012102 (2008).
[3] J. Hlinka, T. Ostapchuk, D. Nuzhnyy, J. Petzelt, P. Kuzel, C. Kadlec, P. Vanek, I. Ponomareva, and L. Bellaiche, Phys. Rev. Lett. **101**, 167402 (2008).
[4] A. B. Sushkov, M. Mostovoy, R. V. Aguilar, S.-W. Cheong, and H. D. Drew, Journal of Physics: Condensed Matter **20**, 434210 (10pp) (2008).
[5] A. Pimenov, A. M. Shuvaev, A. A. Mukhin, and A. Loidl, Journal of Physics: Condensed Matter **20**, 434209 (10pp) (2008).
[6] A. Pimenov, A. Shuvaev, A. Loidl, F. Schrettle, A. A. Mukhin, V. D. Travkin, V. Y. Ivanov, and A. M. Balbashov, Phys. Rev. Lett. **102**, 107203 (2009).
[7] I. Ponomareva and L. Bellaiche, Phys. Rev. Lett. **101**, 197602 (2008).
[8] C. v. Korff Schmising, M. Bargheer, M. Kiel, N. Zhavoronkov, M. Woerner, T. Elsaesser, I. Vrejoiu, D. Hesse, and M. Alexe, Phys. Rev. Lett. **98**, 257601 (2007).
[9] I. Grinberg, Y.-H. Shin, and A. M. Rappe, Phys. Rev. Lett. **103**, 197601 (2009).
[10] P. A. Fleury, J. F. Scott, and J. M. Worlock, Phys. Rev. Lett. **21**, 16 (1968).
[11] J. Petzelt and V. Dvorak, J. Phys. C **9**, 1571 (1976).
[12] D. Bäuerle and A. Pinczuk, Solid State Communications **19**, 1169 (1976).
[13] M. Deluca, H. Fukumura, N. Tonari, C. Capiani, N. Hasuike, K. Kisoda, C. Galassi, and H. Harima, J. Raman Spectrosc., n/a. doi: 10.1002/jrs.2714.
[14] I. A. Kornev, L. Bellaiche, P.-E. Janolin, B. Dkhil, and E. Suard, Phys. Rev. Lett. **97**, 157601 (2006).
[15] W. Zhong, D. Vanderbilt, and K. M. Rabe, Phys. Rev. Lett. **73**, 1861 (1994).
[16] W. Zhong, D. Vanderbilt, and K. M. Rabe, Phys. Rev. B **52**, 6301 (1995).
[17] L. Bellaiche, A. García, and D. Vanderbilt, Phys. Rev. Lett. **84**, 5427 (2000).
[18] L. Bellaiche and D. Vanderbilt, Phys. Rev. B **61**, 7877 (2000).
[19] P. Hohenberg and W. Kohn, Phys. Rev. **136**, B864 (1964).
[20] B. Jaffe, W. Cook, and H. Jaffe, *Piezoelectric Ceramics* (Academic Press, London, 1971).
[21] B. Noheda, L. Wu, and Y. Zhu, Phys. Rev. B **66**, 060103 (2002).
[22] B. Noheda, D. E. Cox, G. Shirane, R. Guo, B. Jones, and L. E. Cross, Phys. Rev. B **63**, 014103 (2000).
[23] J. M. Caillol, D. Levesque, and J. J. Weis, J. Chem. Phys. **85**, 6645 (1986).
[24] C. Domb and M. S. Green (editors), *Phase transitions and Critical Phenomena*, vol. I-V (Academic Press, New York, 1972).
[25] V. Sivasubramanian, V. R. K. Murthy, B. Viswanathan, and M. Sieskind, Journal of Physics: Condensed Matter **8**, 2447 (1996).
[26] E. Buixaderas, S. Kamba, and J. Petzelt, Ferroelectrics **308**, 131 (2004).
[27] F. Gervais, *Infrared and Millimeter Waves*, vol. 8 (Academic, New York, 1983).
[28] C. Cohen-Tannoudji, B. Diu, and F. Laloe, *Quantum Mechanics*, vol. I (Hermann, Paris and John Wiley and sons, New York, 1977).
[29] The order parameter of AFD motions is defined as $\langle \boldsymbol{\omega} \rangle_R = \frac{1}{N} \sum_i \boldsymbol{\omega}_i \left(-1\right)^{n_x(i)+n_y(i)+n_z(i)}$, where $\boldsymbol{\omega}_i$ characterizes the AFD distortion in unit cell i, where the sum runs over the N sites i and $n_\alpha\left(i\right)$ are integers locating the cell i.
[30] These two natural frequencies are associated with the two peaks of Fig. 2 (c). We also check that such extracted resonant frequencies are inversely proportional to the time period associated with the fluctuations of the AFD motions.
[31] Only one single peak with E symmetry is found if one sets to zero the $D_{\alpha\beta\gamma\delta}$ matrix elements of Eq. (2).

Fig. 1: (Color online) Temperature dependence of some dynamical characteristics in $Pb(Zr_{0.55}Ti_{0.45})O_3$ solid solution. Panel (a) shows the ν_r resonant frequency of the lowest-in-frequency dielectric peaks for any temperature, as well as, the resonant frequency of $\varepsilon_{x,x}^{\mathrm{AFD}}(\nu)$ for temperature above 200K (denoted as "AFD mode") found in our simulations. The solid lines represent fittings by square-root laws (i.e., $\nu_r \sim |T - T_c|^{1/2}$) of the resonant frequency of the $E\,(1\mathrm{TO})$ mode and of the soft-mode above T_C. Panel (b) displays the electric dipole spectral weight (extracted from the dielectric response) of different modes (see text).

Fig. 2: (Color online) Complex responses of $Pb(Zr_{0.55}Ti_{0.45})O_3$ solid solution in the $20 - 100\,\mathrm{cm}^{-1}$ frequency range, at different temperatures. Panel (a) and (b) display the real and imaginary part of the $\varepsilon_{x,x}(\nu)$ dielectric response, respectively. Panel (c) shows the imaginary part of the AFD-related $\varepsilon_{x,x}^{\mathrm{AFD}}(\nu)$ function of Eq. (3). The displayed data correspond to a fit of the raw data by two classical damped harmonic oscillator (except at and above $T = 200\,\mathrm{K}$, where we use a single oscillator because of the quality of the fit)[26,27]. The data for 50 K, 75 K, 100 K, 150 K, 200 K, and 300 K have been vertically shifted in Panel (a), (b) and (c) by 2500, 5000, 7500, 10000,12500 and 15000, respectively in order to distinguish them from the 10 K data.

Fig. 3: (Color online) Resonant frequency (Panel (a)) and relative square of the strength of the oscillator (Panel (b)) of the $E^{(1)}$ and $E^{(2)}$ modes (as extracted from their dielectric peaks). Solid lines in Panels (a) and (b) represent fittings by the eigenvalues and eigenvectors of a 2×2 matrix, respectively. In this matrix, the two diagonal terms are frequencies that linearly depend on the magnitude of the electric field (they are indicated by dashed lines in Panel (a)), while the off-diagonal terms are constant frequencies associated with dynamical coupling.

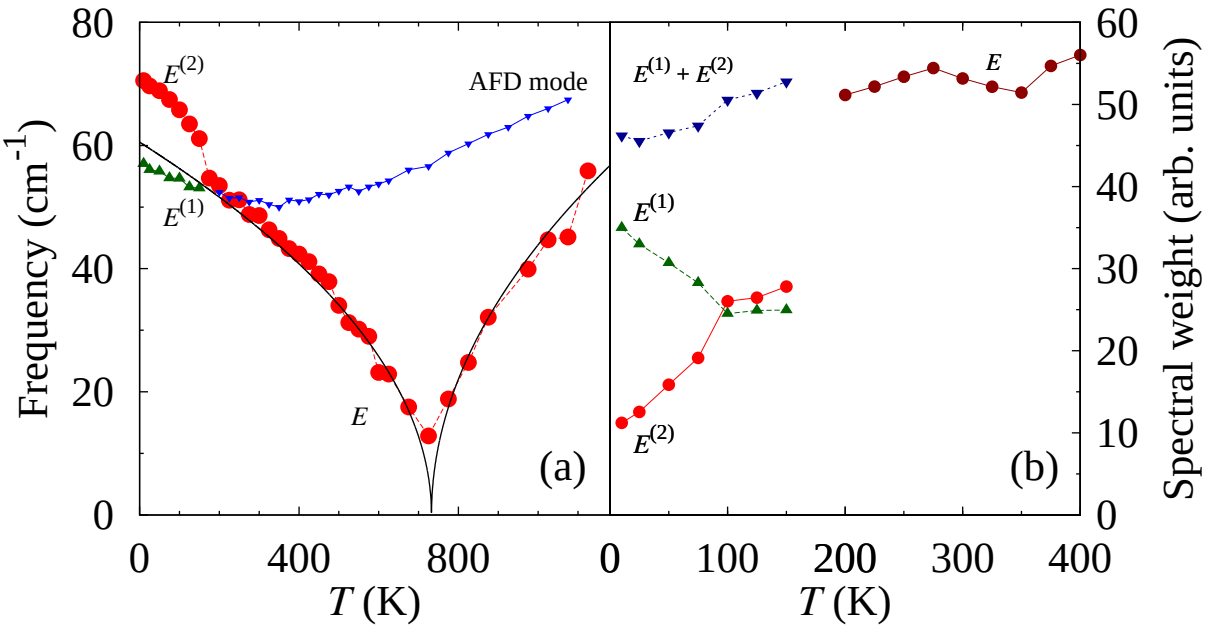

Figure 1 BWR1125 13Dec2010

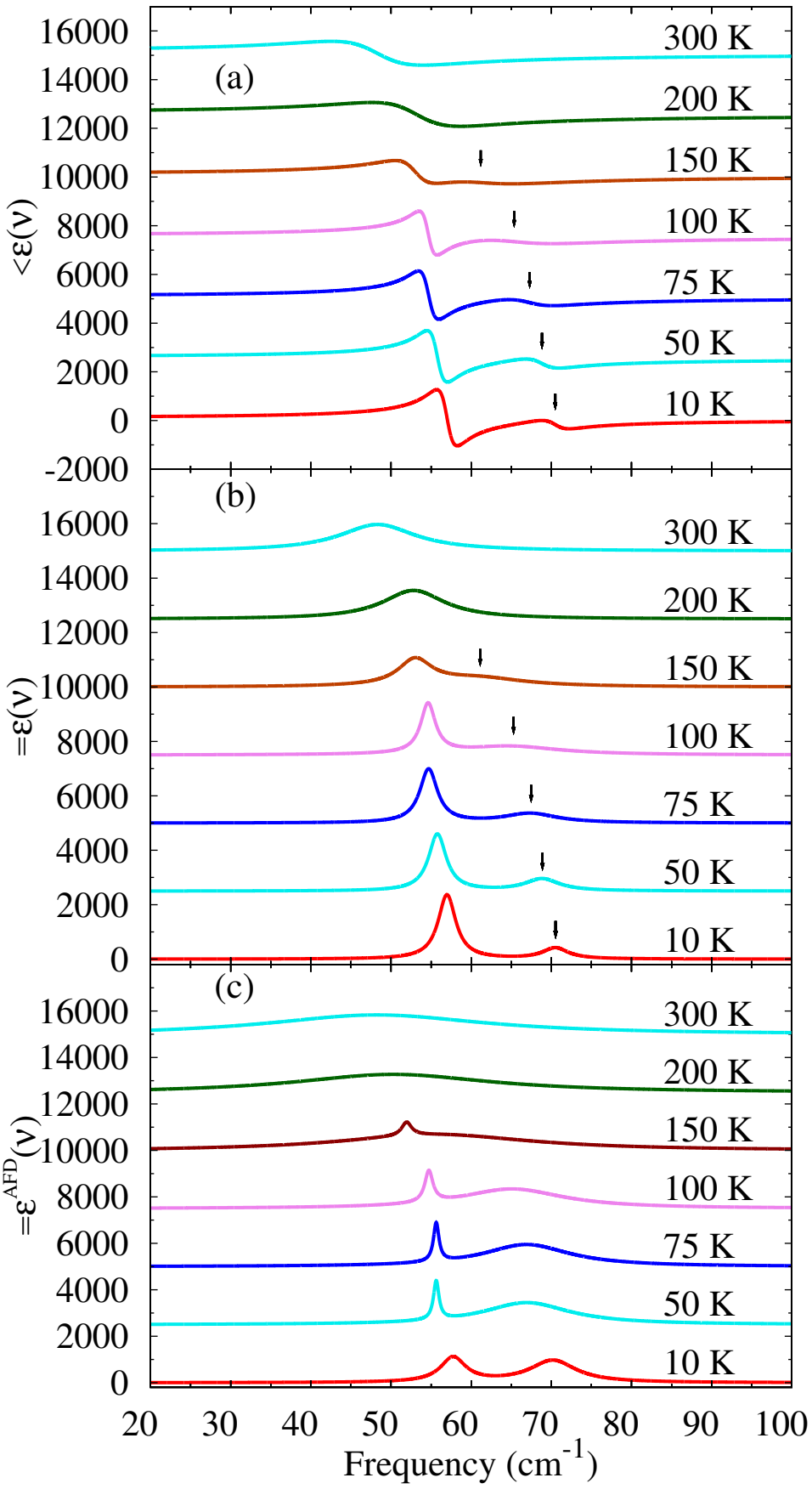

Figure 2 BWR1125 13Dec2010

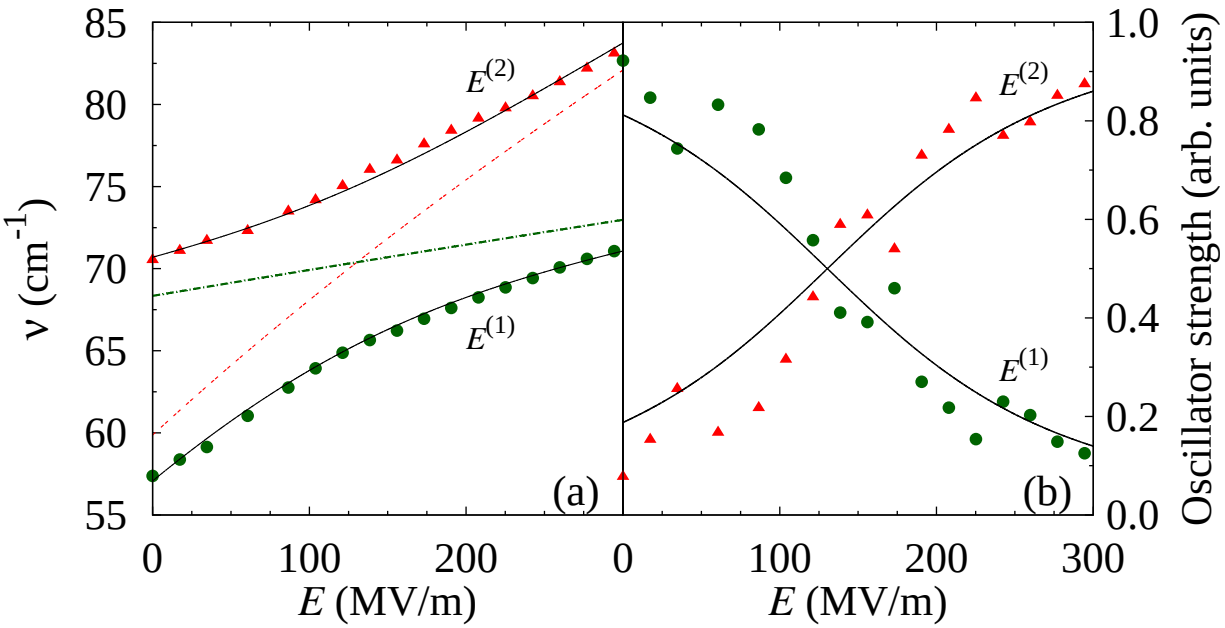

Figure 3 BWR1125 13Dec2010